AD-781 818

A MODEL FOR FIELD ALIGNED SCATTERING (FAS) FROM HEATER MODIFIED IONOSPHERE

Pendyala B. Rao, et al

Raytheon Company

Prepared for:

Rome Air Development Center
Defense Advanced Research Projects Agency

February 1974

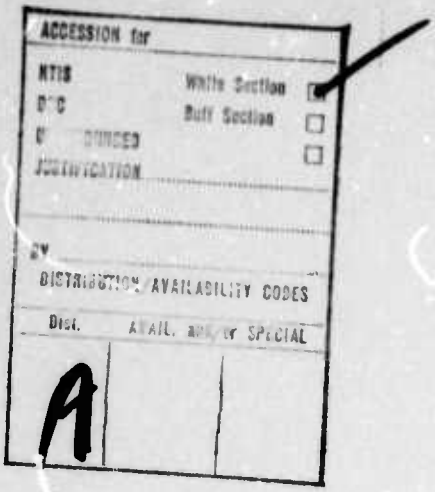

If this copy is not needed, return to RADC (OCSE/R. Schneible) GAFB, NY 13441.

UNCLASSIFIED

SECURITY CLASSIFICATION OF THIS PAGE (When Data Entered)

REPORT DOCUMENTATION PAGE

READ INSTRUCTIONS BEFORE COMPLETING FORM

1. REPORT NUMBER: RADC-TR-74-114, Part 1	2. GOVT ACCESSION NO.
3. RECIPIENT'S CATALOG NUMBER: AD-781818	
4. TITLE (and Subtitle): A Model for Field Aligned Scattering (FAS) from Heater Modified Ionosphere	5. TYPE OF REPORT & PERIOD COVERED: Technical Report January 1973-February 1974
	6. PERFORMING ORG. REPORT NUMBER: 2
7. AUTHOR(s): Pendyala B. Rao and George D. Thome	8. CONTRACT OR GRANT NUMBER(s): F30602-73-C-0154
9. PERFORMING ORGANIZATION NAME AND ADDRESS: Raytheon Company, Sudbury, Massachusetts 01776	10. PROGRAM ELEMENT, PROJECT, TASK AREA & WORK UNIT NUMBERS: Ivory Coral Model Development
11. CONTROLLING OFFICE NAME AND ADDRESS: Defense Advanced Research Projects Agency, Arlington, Va. 22217	12. REPORT DATE: February 1974
	13. NUMBER OF PAGES: 40
14. MONITORING AGENCY NAME & ADDRESS (if different from Controlling Office): Rome Air Development Center, Richard A. Schneible (315) 330-3415, GAFB, N. Y. 13441	15. SECURITY CLASS. (of this report): UNCLASSIFIED
	15a. DECLASSIFICATION/DOWNGRADING SCHEDULE: N/A

16. DISTRIBUTION STATEMENT (of this Report)

DISTRIBUTION STATEMENT A
Approved for public release;
Distribution Unlimited

17. DISTRIBUTION STATEMENT (of the abstract entered in Block 20, if different from Report)

Same

18. SUPPLEMENTARY NOTES

This Report is Part I of a Series of Three Reports

19. KEY WORDS (Continue on reverse side if necessary and identify by block number)

Field Aligned Scattering, Heater Modified Ionosphere, Model of Irregularities

20. ABSTRACT (Continue on reverse side if necessary and identify by block number)

(S) This paper describes the current status in the development of the 'on frequency' scattering model. The presentation adopts a format that is intended to orient the model toward eventual application for systems evaluation. The physical description of the scattering medium which constitutes a basic component to the model is derived from the observations currently at hand. The radar scattering pro-

DD FORM 1 JAN 73 1473 EDITION OF 1 NOV 65 IS OBSOLETE

UNCLASSIFIED

SECURITY CLASSIFICATION OF THIS PAGE (When Data Entered)

perties of the disturbance are described physically by presenting the concepts of aspect sensitivity and surface of specularity for scattering by way of an optical analogy. The mathematical part contains two levels of sophistication in the model treatment. The simpler approach offers an approximate analytic solution and thereby a first-order systems evaluation capability without resorting to a complex computer code. Finally, a flow chart is given for computer adaptation of the scattering model in its general form.

A MODEL FOR FIELD ALIGNED SCATTERING (FAS) FROM HEATER MODIFIED IONOSPHERE

Pendyala B. Rao
George D. Thome

Contractor: Raytheon Company
Contract Number: F30602-73-C-0154
Effective Date of Contract: 15 January 1973
Contract Expiration Date: 28 February 1974
Amount of Contract: $217,661.00
Program Code Number: 3E20

Principal Investigator: G. D. Thome
Phone: 617 443-9521

Project Engineer: Vincent J. Coyne
Phone: 315 330-3141

Contract Engineer: Richard A. Schneible
Phone: 315 330-3085

This research was supported by the Defense Advanced Research Projects Agency of the Department of Defense and was monitored by Richard Schneible RADC (OCSE), GAFB, NY 13441 under Cont F30602-73-C-0154.

PUBLICATION REVIEW

This technical report has been reviewed and is approved.

Richard A. Schneible

RADC Project Engineer

ABSTRACT (U)

This paper describes the current status in the development of the on-frequency scattering model. The presentation adopts a format that is intended to orient the model toward eventual application for systems evaluation. The physical description of the scattering medium which constitutes a basic component to the model is derived from the observations currently at hand. The radar scattering properties of the disturbance are described physically by presenting the concepts of aspect sensitivity and surface of specularity for scattering by way of an optical analogy. The mathematical part contains two levels of sophistication in the model treatment. The simpler approach offers an approximate analytic solution and thereby a first-order systems evaluation capability without resorting to a complex computer code. Finally, a flow chart is given for computer adaptation of the scattering model in its general form.

CONTENTS (U)

LIST OF ILLUSTRATIONS

LIST OF ILLUSTRATIONS

1. INTRODUCTION(U)

A model for the 'on frequency' field aligned scattering has been developed on the basis of the work performed to date by all the members involved in the modeling task. The model is intended primarily for use in systems applications and its presentation format has been adopted accordingly. This paper constitutes an attempt to present the model in a form that would best meet its intended objective and it is hoped that it reflects the consensus of the modeling group.

The formulation of the model begins with a physical description of the scattering medium which specifies the dimensions of the disturbance, wave number spectrum of the density fluctuations and a yield model relating the fluctuation intensity to the heater power density. The characterization of the medium is an important aspect of the modeling task and we strive in this presentation to see that it is consistent with all the available observations to the best possible extent. It is followed by a description of the radar properties of the disturbed volume where the concepts of aspect sensitivity and surface of specularity are introduced as well as the underlying principle relating the bistatic and monostatic scattering geometries. The mathematical component of the model is presented in two parts, each representing a different degree of sophistication in computing the total radar cross section. The first part is concerned with a general case where a bistatic geometry and a realistic yield model are considered and it involves a numerical approach. The second part, considering a monostatic geometry and an idealized yeild model, offers an analytic solution. This case is of interest since a general bistatic radar problem can be reduced to an equivalent monostatic case and can be evaluated to a first order without resorting to a complex computer program. Finally a schematic flow diagram is given for computer adaptation of the model.

2. PHYSICAL DESCRIPTION OF THE SCATTERING MEDIUM (U)

2A. Dimensions of the Disturbance (U)

The physical model of the disturbance generated by the Platteville heater is shown pictorially in figure 1. The disturbed volume containing the small electron density fluctuations responsible for the field aligned scattering of the radio waves is a diffuse region centered above the heater at the height where the heater frequency equals the local ionospheric plasma frequency. The strength of the irregularities falls off above and below this altitude with a Gaussian scale

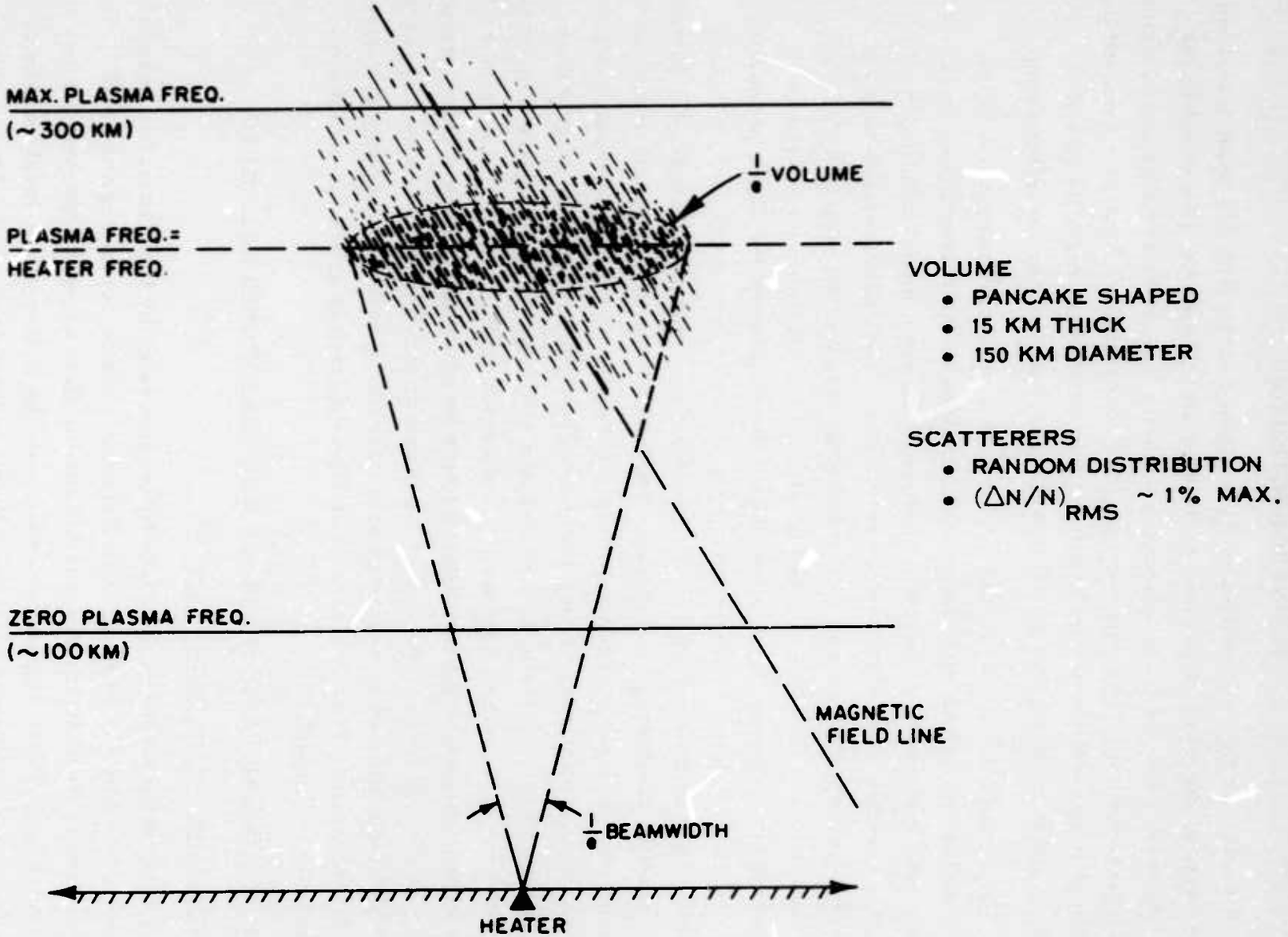

Figure 1. Physical Model of the Volume Containing Electron-Density Irregularities Responsible for "On-Frequency" Field Aligned Scattering

length of 7.5 Km (15 Km between 1/e points). The lateral dimensions of the volume are set by the width of the heater antenna beam: for Platteville heater this sets the Gaussian radius of the disturbed volume at 50 Km (100 Km between 1/e points) for a heater reflection height of 240 Km. The disturbed volume can thus be visualized as a flat pancake - shaped region with diffuse boundaries. At the center of the disturbed volume the rms intensity of the electron density fluctuations is typically 1 to 1.5% when the heater is operating at its full power of 1.9 Mw. The physical description of the distrubance presented here has been arrived at primarily by requiring the resulting scattering model to be consistent with the radar observations.

2B. Wave Number Spectrum: (U)

(U) The wave number spectrum of the density fluctuations of the scattering medium is related to the backscatter coefficient σ_v as (Booker, 1956)[1]:

$$\sigma_v = \frac{\pi^2}{\lambda_N^4} \left(\frac{\Delta N}{N}\right)^2 \quad P\,(2K\ell, 2Km, 2Kn) \tag{1}$$

In the case of strongly aspect-sensitive scatter, the three dimensional wave number spectrum can be written in separable form as (Minkoff, 1973)[2]:

$$P(K_x, K_y, K_z) = P_\perp (K_x, K_y)\, P_{\parallel} (K_z) \tag{2}$$

Where the two components are defined in terms of the corresponding spatial correlation function as

$$P_\perp (K_x, K_y) = \int_{-\infty}^{\infty}\int_{-\infty}^{\infty} R_\perp (x, y) \cdot \exp\left\{-i(K_x x + K_y y)\right\} dx\, dy \tag{3}$$

and

$$P_{\parallel} (K_z) = \int_{-\infty}^{\infty} R_{\parallel} (z) \cdot \exp(-iK_z z)\, dz \tag{4}$$

The density fluctuations are assumed to be axially symmetric around the magnetic field and consequently the transverse correlation function $R_\perp(x, y)$ is dependent only on the radial distance; that is $R_\perp(x, y) = R_\perp(\rho)$, where $\rho = (x^2 + y^2)^{\frac{1}{2}}$. This simplification and the use of cylindrical coordinates lead to the familiar Hankel transform relation:

$$P_\perp (K_\perp) = 2\pi \int_0^{\infty} \rho\, R_\perp (\rho)\, J_o (\rho K)\, d\rho \tag{5}$$

where

$$K_{\perp}^2 = K_x^2 + K_y^2$$

When we are interested only in fairly small values of ψ, the magnetic aspect angle, we may use the following approximations:

$$\ell^2 + m^2 \approx 1 \quad \text{and } n \approx \psi$$

Hence

$$P_{\perp}(2K\ell, 2Km) = P_{\perp}(2K) \tag{6a}$$

and

$$P_{\parallel}(2Kn) = P_{\parallel}(2K\psi) \ . \tag{6b}$$

using a Gaussian spatial correlation for the density fluctuations along the magnetic field, that is $R_{\parallel}(z) = \exp(-z^2/2L^2)$, we obtain

$$P_{\parallel}(2K\psi) = (2\pi)^{\frac{1}{2}} L \exp(-2K^2L^2\psi^2) \tag{7}$$

using the equations (6a) and (7) we now seek to obtain a relation between σ_T, the total radar cross section and $P_{\perp}(2K)$ in order to determine the transverse spectrum from the radar measurements.

$$\sigma_T(K) = 4\pi \int_v \sigma_v(K)\, dv$$

$$= \frac{4\pi^3}{4} (2\pi)^{\frac{1}{2}} L\, P_{\perp}(2K) \tag{8}$$

$$\int_{-\infty}^{\infty}\int_{-\infty}^{\infty}\int_{-\infty}^{\lambda_N} \overline{\left(\frac{\Delta N}{N}\right)^2}(x, y, z) \exp\left[\frac{-2K^2L^2z^2}{R^2}\right] dx\, dy\, dz$$

Where $\psi \approx z/R$ substitution was made, R being the range to the scattering volume from the radar.

The intensity of the density fluctuations in a coordinate system (X, Y, Z) centered on the reflectrix above the heater with Z axis vertically up is expressed as:

$$\overline{\left(\frac{\Delta N}{N}\right)^2} = \overline{\left(\frac{\Delta N}{N}\right)_o^2} \exp\left\{-\frac{(X^2 + Y^2)}{W^2} - \frac{Z^2}{A^2}\right\} \tag{9}$$

Where $\overline{(\Delta N/N)_o^2}$ is the intensity at the origin, W and A are the Gaussian radii of the disturbance in horizontal and vertical directions respectively. $\overline{(\Delta N/N)^2}$ is expressed in the computational system (x, y, z) by means of a coordinate transformation. The computational system is centered on the specular surface with its origin right above the heater and the z axis perpendicular to the surface. The transformation is effected by

$$X = x \cos\theta + z \sin\phi$$

$$Y = y$$

$$Z = -x \sin\theta + z \cos\theta + D$$

Where θ is the tilt of the specular surface from horizontal and D is the vertical mismatch of the specular surface from the reflectrix. Using the above form for $\overline{(\Delta N/N)^2}$, the integral in Equation (8) is solved to obtain (Pendyala and Thome, 1972)[3]:

$$\sigma_T(K) = \left\{ \frac{4\pi^5 W^2 R \overline{(\Delta N/N)_o^2}}{\lambda_N^4 \left[\cos^2\theta + \frac{W^2}{A^2} \sin^2\theta\right]} \right\}^{\frac{1}{2}} \frac{P_\perp(2K)}{K} \qquad (10)$$

Since $P_\perp(K_T)$, where $K_T = 2K$, must satisfy the normalization:

$$R_\perp(0) = 1 = \frac{1}{2\pi} \int_0^\infty K_T \, P_\perp(K_T) \, dK_T \qquad (11)$$

it follows from Equation (10) that

$$\overline{(\Delta N/N)_o^2} = \left\{ \frac{\lambda_N^4 \left[\cos^2\theta + (W^2/A^2)\sin^2\theta\right]^{\frac{1}{2}}}{2\pi^6 W^2 R} \right\} \int_0^\infty K^2 \, \sigma_T(K) \, dk \qquad (12)$$

The intensity of the density fluctuation is calculated by using the radar observations of σ_T shown in Figure 2 to evaluate the integral in Equation (12). The numerical evaluation of the integral does not include contribution from radar frequencies below 20 MHz. We obtain

$$(\Delta N/N)_o \text{ RMS} \approx 1\%$$

when the following parameters are used.

$\lambda_N = 54M$ $\qquad$ W = 50 Km

$\theta = 10^o$ $\qquad$ A = 7.5 Km

R = 900 Km

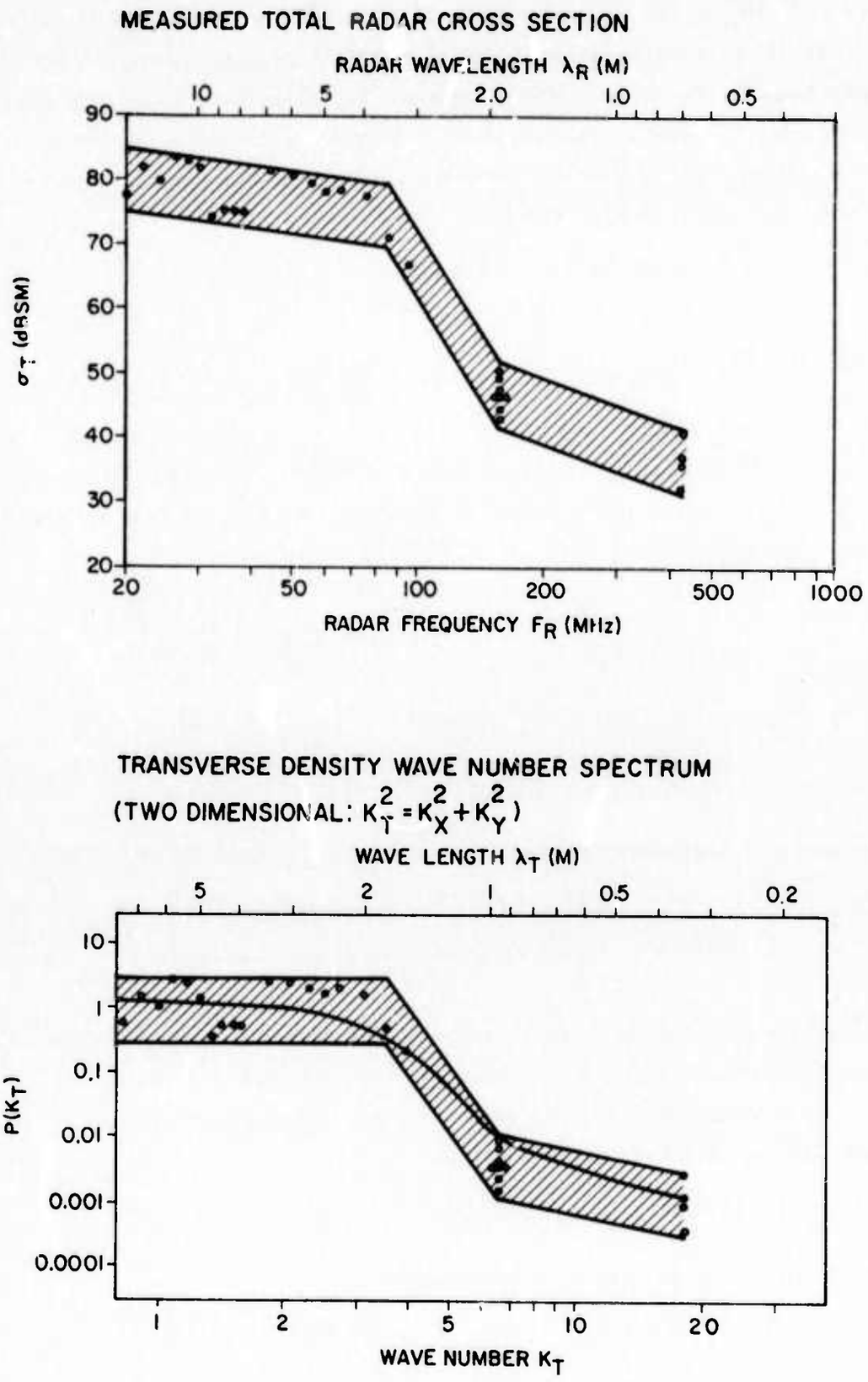

Figure 2. Measurement of Total Radar Cross Section and the Derived Transverse Wavenumber Spectrum of Density Fluctuations

The transverse spectrum derived from the radar observations by means of Equation (10) is also shown in Figure 2. It is a three segment spectrum such that

$$\begin{aligned} P_{\perp}(K_T) &= 0.4 && (0.8 \leq K_T \leq 3.3) \\ &= 0.8 \times 10^{4} K_T^{-8.3} && (3.3 \leq K_T \leq 6.6) \\ &= 0.8 \times 10^{-2} K_T^{-1.1} && (6.6 \leq K_T \leq 18.23) \end{aligned}$$

The curve drawn through the hatched region of the wave number spectrum represents a double- Gaussian fit of the form:

$$P_{\perp}(K_T) = 2\pi \left\{ \alpha T_1^2 \left[\exp - \tfrac{1}{2} K_T^2 T_1^2 \right] + (1-\alpha) T_2^2 \left[\exp - \tfrac{1}{2} K_T^2 T_2^2 \right] \right\} \quad (13)$$

Where α is a constant and T_1 and T_2 are two dominant transverse correlation distances of the density fluctuations.

2C. Yield Model [$\overline{(\Delta N/N)^2}$ dependence on heater power density]

One of the important elements of the scattering model is the density fluctuation intensity $\overline{(\Delta N/N)^2}$. A model as to how this quantity depends on the heater power density, referred to as yield model, is presented in this section. There are two ways to arrive at the desired model on the basis of the radar observations relating the total cross section σ_T to the heater power P_H. One involves performing a numerical inversion of the observed radar data to obtain the required solution. The other method is indirect, in that a model will be assumed to start with, and tested for its validity by synthesizing the radar cross sections and comparing them with the measurements. The second method has been adopted here since it is relatively simpler. It is assumed in the analysis given here that the heater power affects only the intensity and not the spectrum of the density fluctuations.

Radar observations from PS V show a wide variability in the radar cross section yeild as a function of the heater power. The results may be classified into two types: one revealing a constant slope and the other a variable slope with the heater power. Bulk of the measurements falls into first category and

they are shown in the form of scatter plot in figure 3. The cross section has a power law dependence on the heater power with the exponent ranging over 0.3 to 1 with a median value of about 0.65. In the case of SRI data, it was found that lower slopes are in general associated with the conditions when the heater is operating close to the critical frequency. For these measurements of constant slope, the yield model relating $(\Delta N/N)^2$ to the heater power density is the same as that relating the cross section to the heater power. In some instances, the second type of behavior with variable slope is noted although the conditions under which this happens are not yet identified. Influenced by the observed behavior, we have started with a simple two-step model with density fluctuations increasing linearly with power density up to a certain level and 0.33 times as rapidly above that level (Figure 4). Based on the model, the computation of the normalized total cross section as a function of the heater power proceeds as follows:

Let the heater antenna pattern be Gaussian so that the power density distribution on the reflectrix is

$$P_D = P_o \exp\left[-(R/W)^2\right] \tag{14}$$

Where P_o is the power density at the center, R is the radial distance and W is the Gaussian radius of the antenna beam. Let P_S be the power density level above which the density fluctuation power law dependence changes from 1 to 0.33. When the peak power density P_o is greater than P_S, the radius of the region where the change occurs in the power law is given as

$$R_c^2 = W^2 \ln (P_o/P_S) \tag{15}$$

The distribution of the density fluctuations on the reflectrix, when normalized to 1 at the center for maximum heater power, is

$$\overline{(\Delta N/N)^2}_R = \exp\left[-0.33\,(R/W)^2\right] \qquad (R \leq R_c)$$

$$= \exp\left[-0.33\,(R_c/W)^2\right] \exp\left[-(R^2 - R_c^2)/W^2\right] \qquad (R > R_c)$$

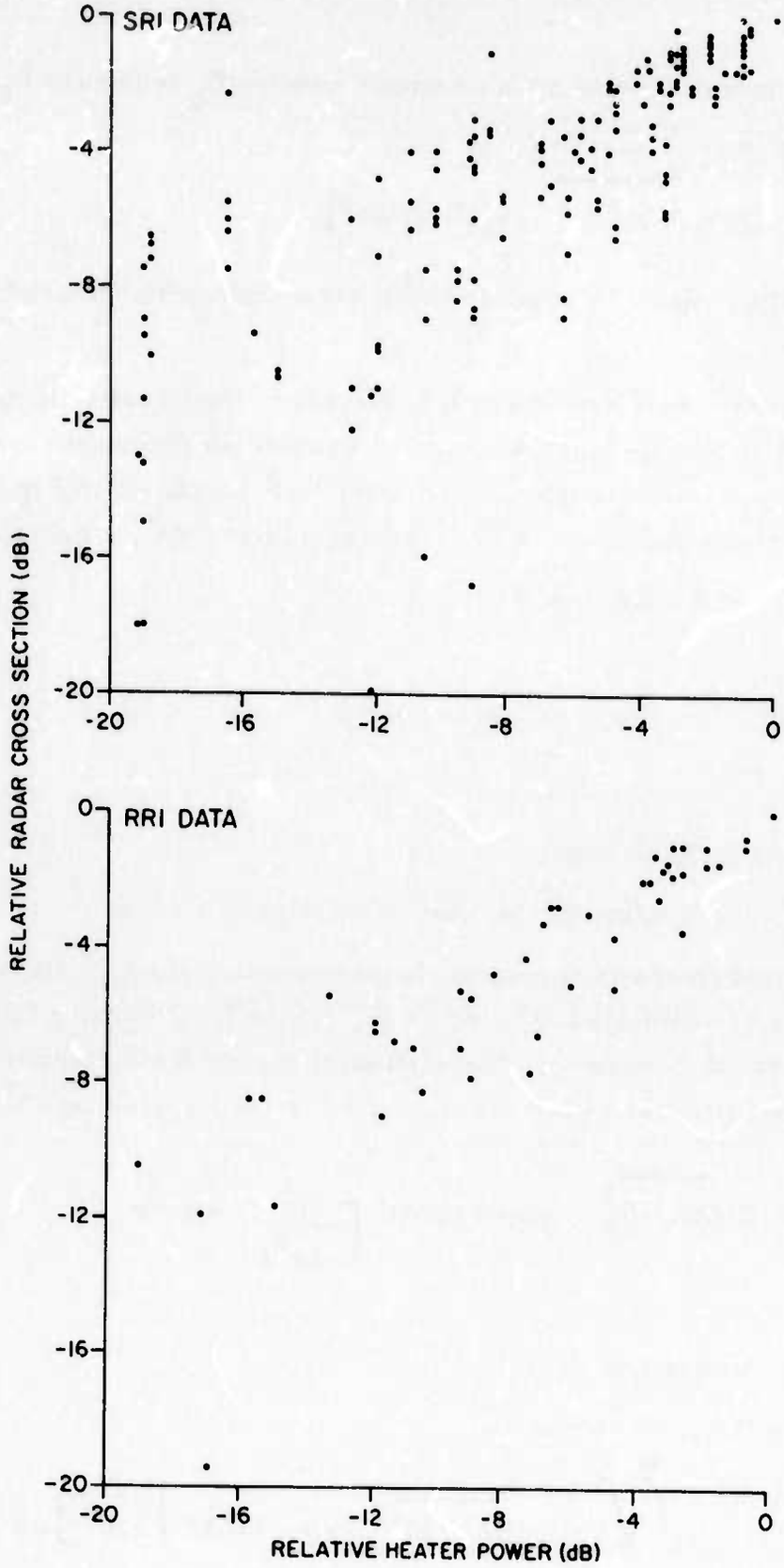

Figure 3. A scatter plot of the yield measurements conducted by SRI and RRI during PS V which reveal a constant power law dependence between radar cross section and heater power on any individual run.

When the heater is operating with on-axis power density P_o less than P_S, then

$$R_c = 0$$

and $$\overline{(\Delta N/N)_R^2} = (P_o/P_S)\ \overline{(\Delta N/N)_S^2}\ \exp\left[-(R/W)^2\right]$$

where $\overline{(\Delta N/N)_S^2}$ is the density fluctuation value associated with the power density P_S.

In order to compute the radar cross section, however, the density fluctuations had to be calculated on the specular surface. Consider an elemental area dA on the reflectrix at some radial distance R and azimuth ϕ as shown in Figure 5. The corresponding elemental area on the specular surface dA′ is given as:

$$dA' = R\, dR\, d\phi/\cos^2\theta$$

and

$$\cos^2\theta = \cos^2\phi\ \cos^2\theta_o + \sin^2\phi$$

where

ϕ = azimuth angle

θ_o = inclination of the specular surface

The density fluctuation intensity tapers off from the reflectrix in a Gaussian manner with a vertical scale size denoted as A. Hence the intensity on dA′ is $\overline{(\Delta N/N)_R^2}\ [\exp - (d/A)^2]$ where d is the vertical distance R tan θ separating dA and dA′. The incremental radar cross section $d\sigma$ contributed by dA′ can be written as:

$$d\sigma = C\ \overline{(\Delta N/N)_R^2}\ \exp - (d/A)^2 \left[\frac{R}{\cos^2\theta}\right] dR\, d\phi \qquad (16)$$

where

C = A constant

Integrating Equation (15), we obtain

$$\sigma_T = C \int_0^{\infty}\int_0^{2\pi} \overline{(\Delta N/N)^2}\ \exp - (d/A)^2 \left[\frac{R}{\cos^2\theta}\right] dR\, d\phi \qquad (17)$$

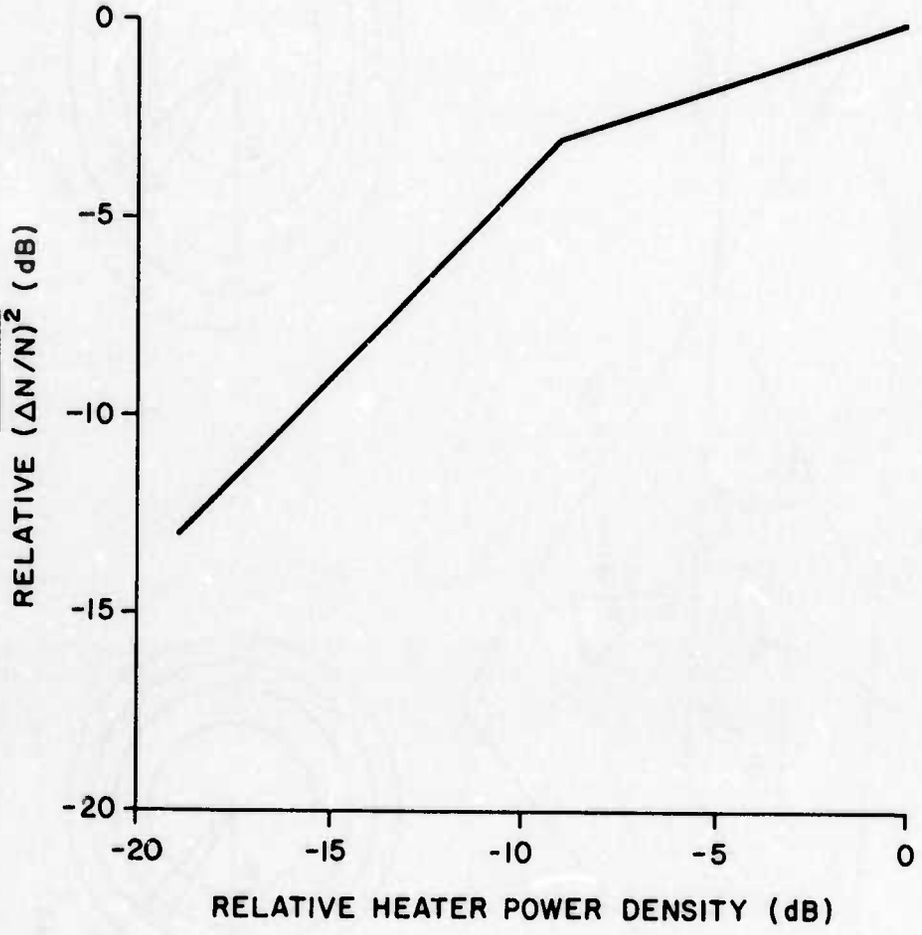

Figure 4. The Two Step Yield Model for $\overline{(\Delta N/N)^2}$ on which the Computations are Based

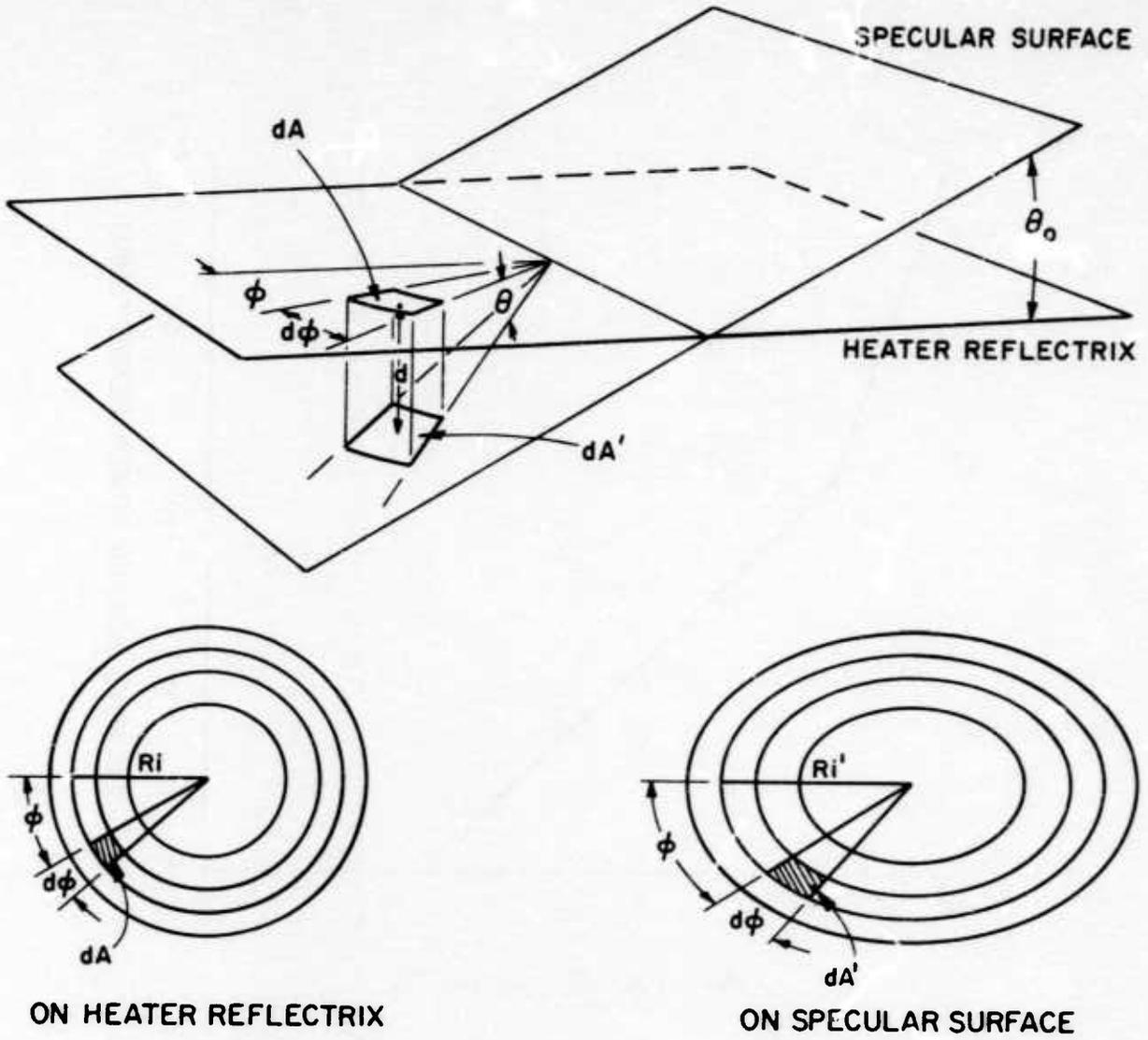

Figure 5. The Specular-Surface/Heater Reflextrix Geometry Adopted in Deriving the Yield Model

The above surface integral is numerically evaluated by dividing the surface into concentric rings as shown in Figure 5. The outermost ring encloses all the area of interest with dimensions twice the Gaussian diameter of the disturbance. The cross section is calculated for different power values relative to its value when the heater is operating at the maximum power. Figure 6 shows a comparison between the synthesized (dashed curve) and the observed cross section dependence on the heater power. Given the uncertainties in the yield measurements, the simple model presented here can be considered adequate to account for the power dependence of the radar cross section. Some caution should, however, be exercised in adopting a simple yield model because of the wide variability seen in the measurements.

3. RADAR PROPERTIES OF THE DISTURBED VOLUME (U)

3A. Aspect sensititivy and the concept of a surface of specularity (U)

The high aspect sensitivity of the scatterers leads to an important modeling concept - the surface of specularity. The importance of the concept is, first of all, that it helps to physically understand the radar results, and secondly, that it reduces the numerical task of computing radar scattering cross sections from a 3-dimensional problem to a 2-dimensional problem. Consider first the optical analog shown in Figure 7. The glass rods are aligned with the earth's field and represent the small field-aligned fluctuations in refractive index caused by heating the ionosphere. The light from the candle flame is partially reflected by the glass rods, and an observer behind the candle sees an image of the flame at the specular point on each rod. If there are many closely spaced rods, the images from each will blend together to form a bright "specularity surface" on which the specular points for all rods lie. The only part of the rod that matters for the observer is the segment that coincides with the specularity surface. The corresponding picture for the radar case is shown in Figure 8. The glass rods have been replaced by the field-aligned electron-density irregularities caused by the heater. In this case, the height where the heater frequency matches the local plasma frequency is well above the specularity surface for the radar and consequently only the weak lower tips of the irregularities are "seen" by the radar. The received signal strength will consequently be weak.

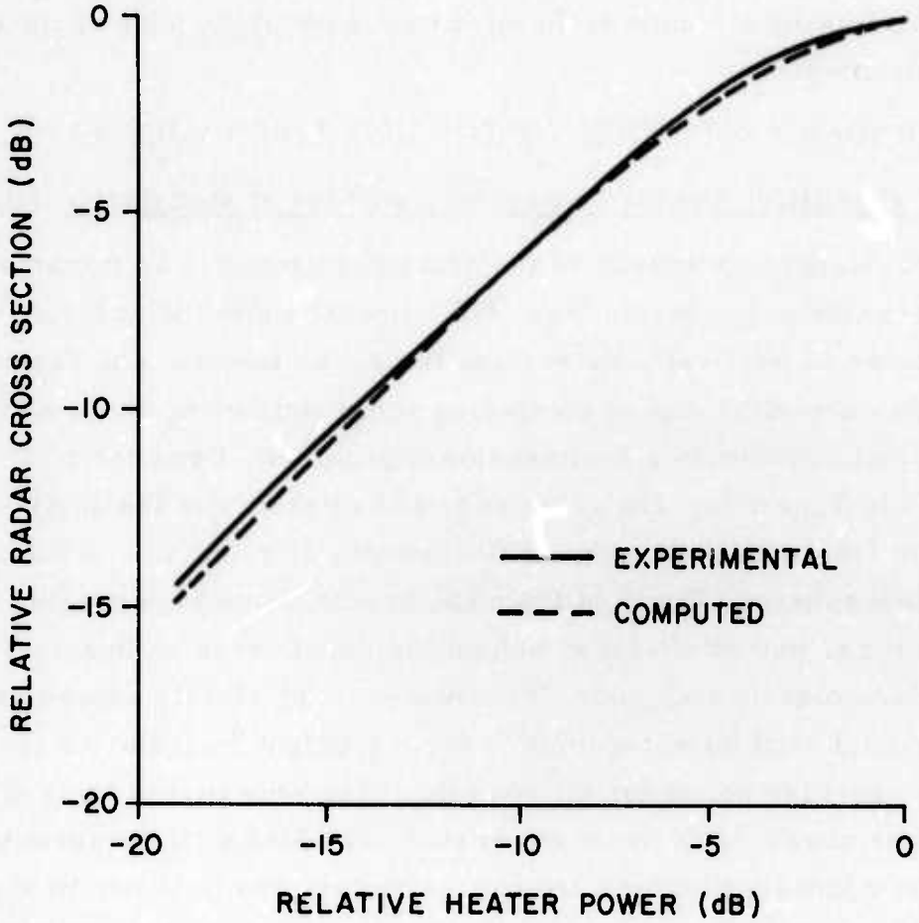

Figure 6. Comparison Between Experimental and Computed Radar Cross-Section Dependence on Heater Power

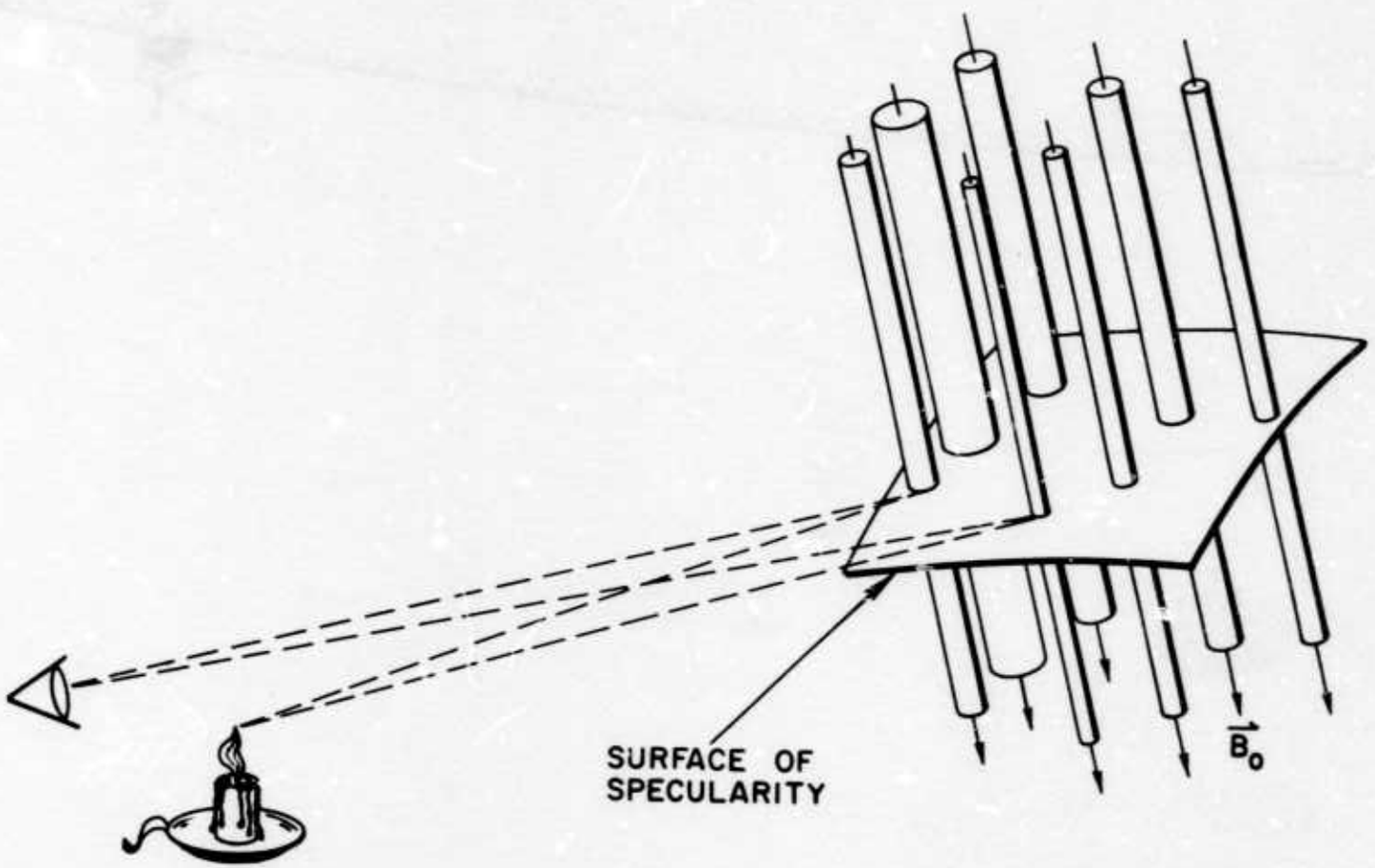

Figure 7. Illustration of the Concept of a Surface of Specularity for Reflections from a Bundle of Closely Spaced Field-Aligned Scatterers (Glass rods) (U)

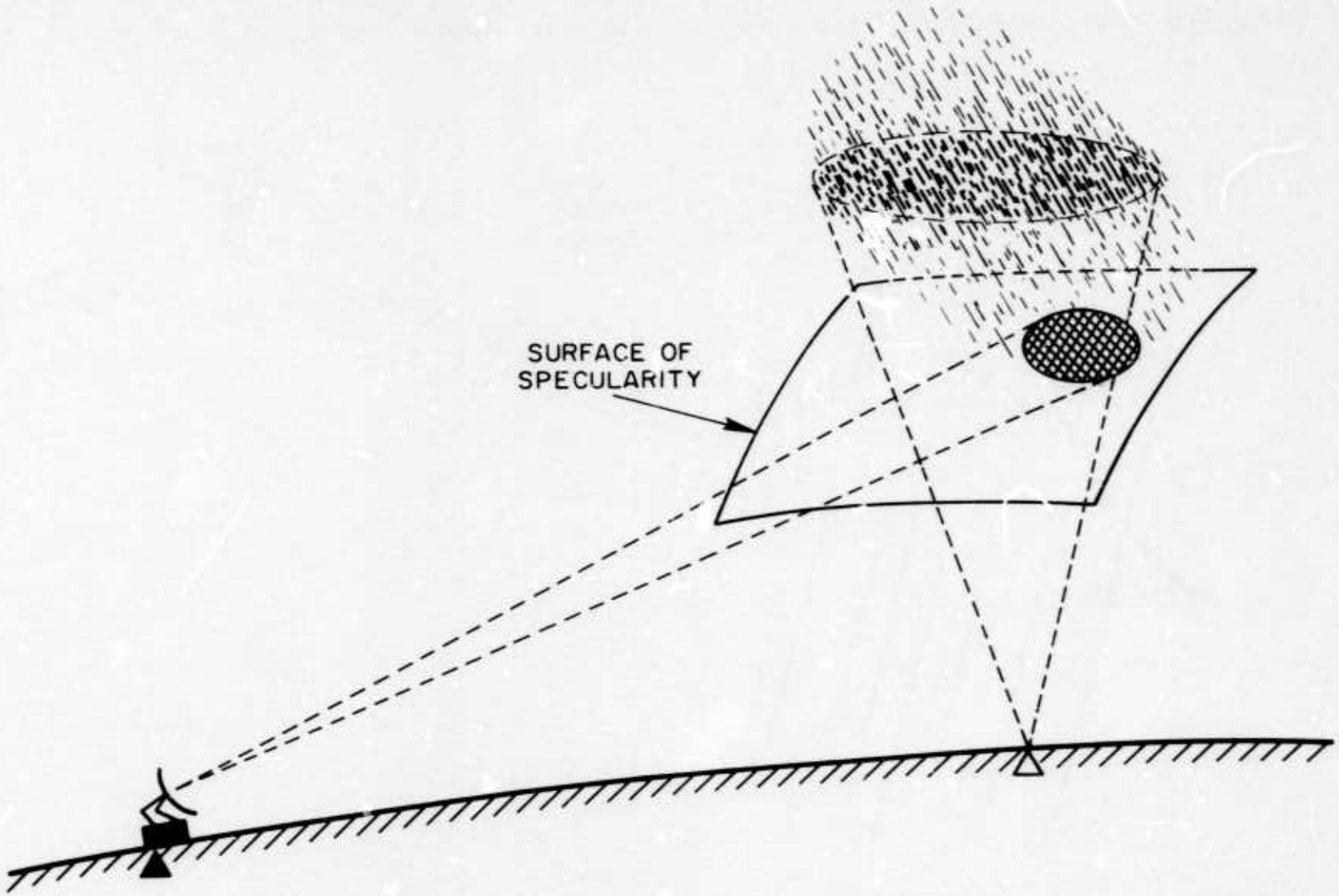

Figure 8. The Surface of Specularity in the Radar Case, illustrating that the observed scatter will be weak when the heater reflection height is poorly matched to the height of the specularity surface

The situation can be improved by lowering the heater frequency (and consequently the height where the heater frequency matches the plasma frequency) till the disturbed volume coincides with the surface of specularity. The concept is qualitatively the same for bistatic as well as for monostatic paths: The procedure is to compute the surface of specularity, given the end points of the path and a model of the earth's field, and then use the strength of the scatterers lying on the surface to compute the effective scattering cross section of the disturbed volume. This converts the computational problem from a volume integration to a surface integration with a corresponding reduction in complexity.

3B. Bistatic Versus Monostatic Scattering Geometries (U)

(U) When the receiver and transmitter of a communications path are separated from each other (bistatic rather than monostatic operation) the scattering properties of the disturbed volume are modified. The principal modification is that the size of the irregularities that support scatter over bistatic paths is larger than the size that supports backscatter at the same frequency. The situation is shown in Figure 9. The Bragg condition for constructive interference says that the spatial Fourier component, which counts in determining the strength of the wave scattered through an angle θ, is the component of spatial wavelength $s = \lambda/2 \sin(\theta/2)$, where λ is the wavelength of the incident radio wave. When this condition is met, the waves scattered from adjacent crests of the spatial Fourier components will differ in phase by exactly one wavelength and thus will add coherently in the direction of interest. Figure 9 Illustrates the fact that the spatial wavelength of interest becomes longer as the path changes from monostatic to bistatic. Since the strength of the spatial frequency spectrum increases monotonically as the wavelength becomes longer (see Figure 3, bottom), the disturbed volume will scatter more strongly over a bistatic path than over a backscatter path, all else being equal.

(U) The "bistatic gain" predicted by the model for a 90° scattering angle is shown in Figure 10. The shaded area shows the range in which backscatter measurements of total radar cross section fall as a function of frequency. The solid "backscatter" curve shows that the model predictions are in agreement with the observations, and the solid "bistatic" curve shows the increase in cross section expected for a 90° scattering angle. Gains of 10 dB or more can be expected, depending on frequency.

BRAGG SCATTERING

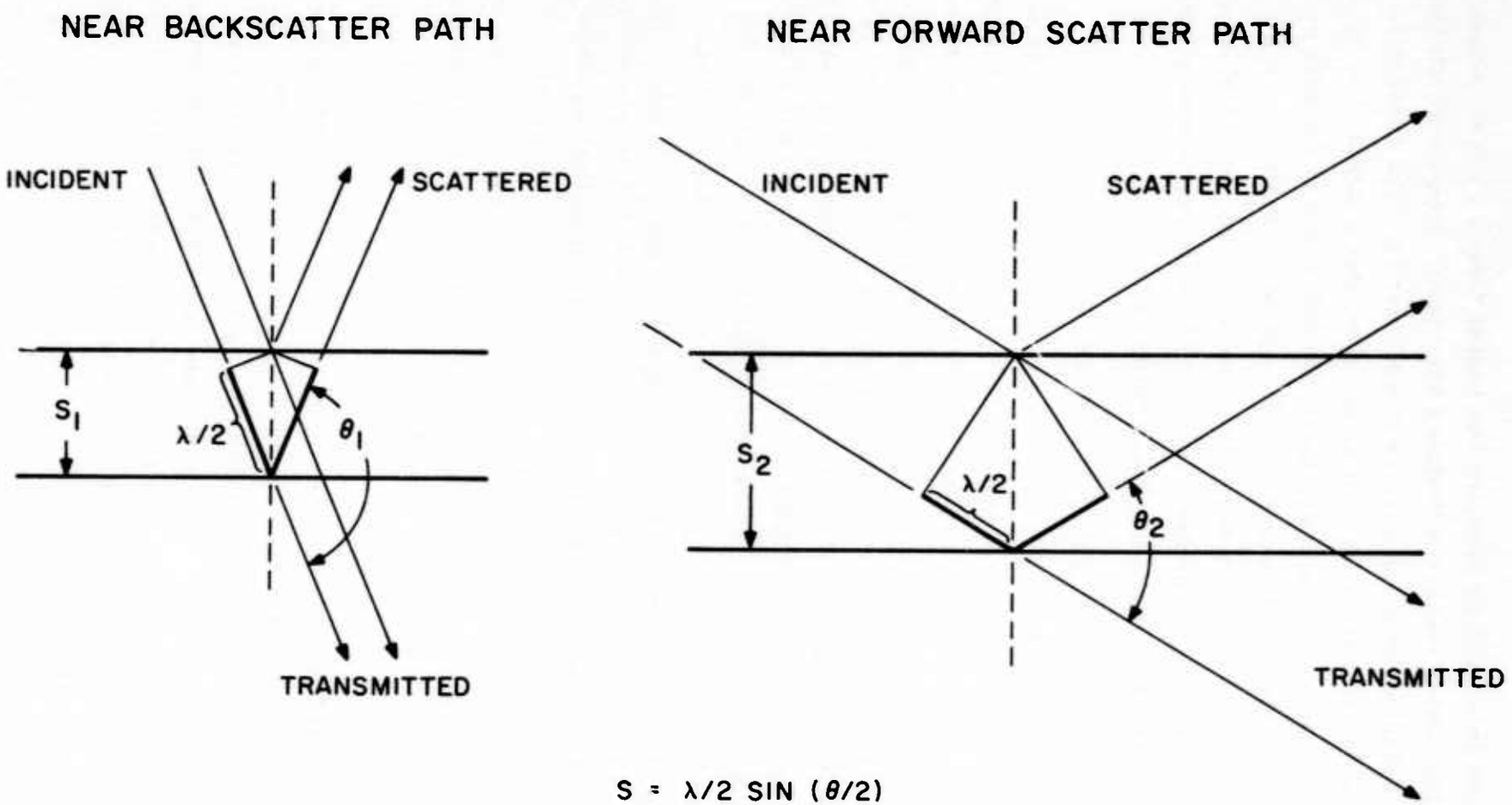

Figure 9. Illustration Showing that the wavelength of the spatial frequency component that controls the strength of the signal scattered through an angle θ increases as the scatter geometry changes from monostatic to bistatic. (Here, λ is the radiowavelength and s is the wavelength of the spatial Fourier component that produces constructive interference in the direction of interest) (U)

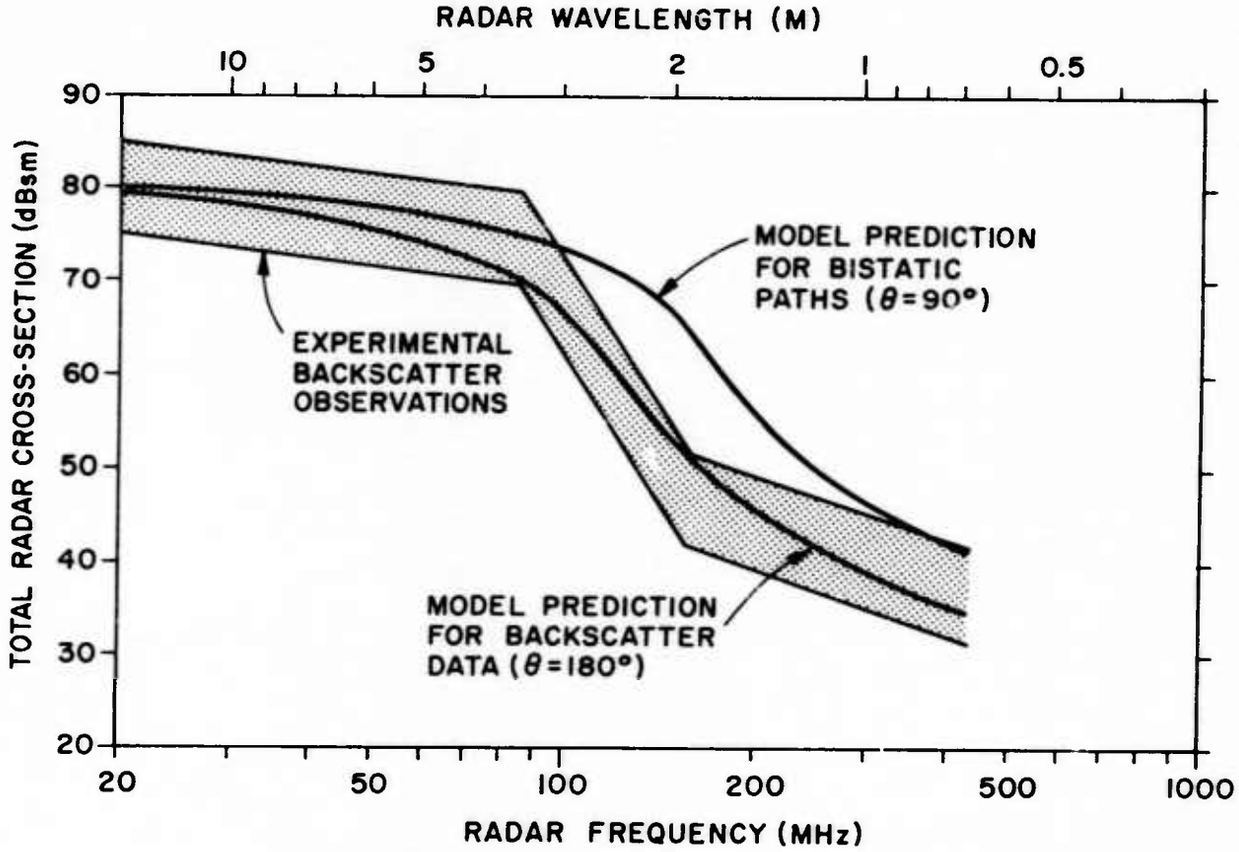

Figure 10. A Comparison between expreimental backscatter measurements of the total radar cross-section of the disturbed volume as a function of frequency (shaded area), model prediction for backscatter (lower solid curve), and model prediction for a 90^{o} bistatic path (upper solid curve)

4. MATHEMATICAL MODEL FOR σ_T (U)

4A. General Case (Bistatic Geometry and Realistic Yield Model) (U)

The formulation of the mathematical model presented here involves basically, the derivation of an expression for the radar cross section per unit area σ_A on the specular surface. The total radar cross section σ_T is computed by numerical evaluation of the surface integral of σ_A. The radar cross section per unit volume σ_v of the scattering medium, which must be integrated along the direction normal to the specular surface to obtain σ_A, is expressed by Booker[1] as:

$$\sigma_v = \frac{\pi^2 \sin^2\chi}{\lambda_N^4} \overline{(\Delta N/N)^2} \; P\left\{K(\ell_2 - \ell_1),\ K(m_2 - m_1),\ K(n_2 - n_1)\right\} \tag{18}$$

where

χ = Angle between incident E vector and the direction of scattering

λ_N = Background plasma wavelength

$(\ell_1, m_1 n_1)$ = Direction cosines of incident wave vector

and

(ℓ_2, m_2, n_2) = Direction cosines of scattered wave vector

Resolving the three dimensional wave number spectrum into parallel and transverse components as before and assuming the spectrum to be cylindrically symmetric, we can write

$$\sigma_v = \frac{\pi^2 \sin^2\chi}{\lambda_N^4} \overline{(\Delta N/N)^2} \; P_\perp\left\{K\left[(\ell_2-\ell_1)^2 + (m_2-m_1)^2\right]^{\frac{1}{2}}\right\} P_\parallel\left\{K(n_2-n_1)\right\} \tag{19}$$

Now let us consider a unit volume at point P above the elemental area dA_j of the specular surface as sketched in Figure 11. The elemental area is located at $(X_i,\ Y_i,\ Z_i)$ in the coordinate system centered on the heater reflectrix and the density fluctuation at this point is

$$\overline{(\Delta N/N)_i^2} = \overline{(\Delta N/N)_{Ri}^2} \exp\left\{-(Zi/A)^2\right\} \tag{20}$$

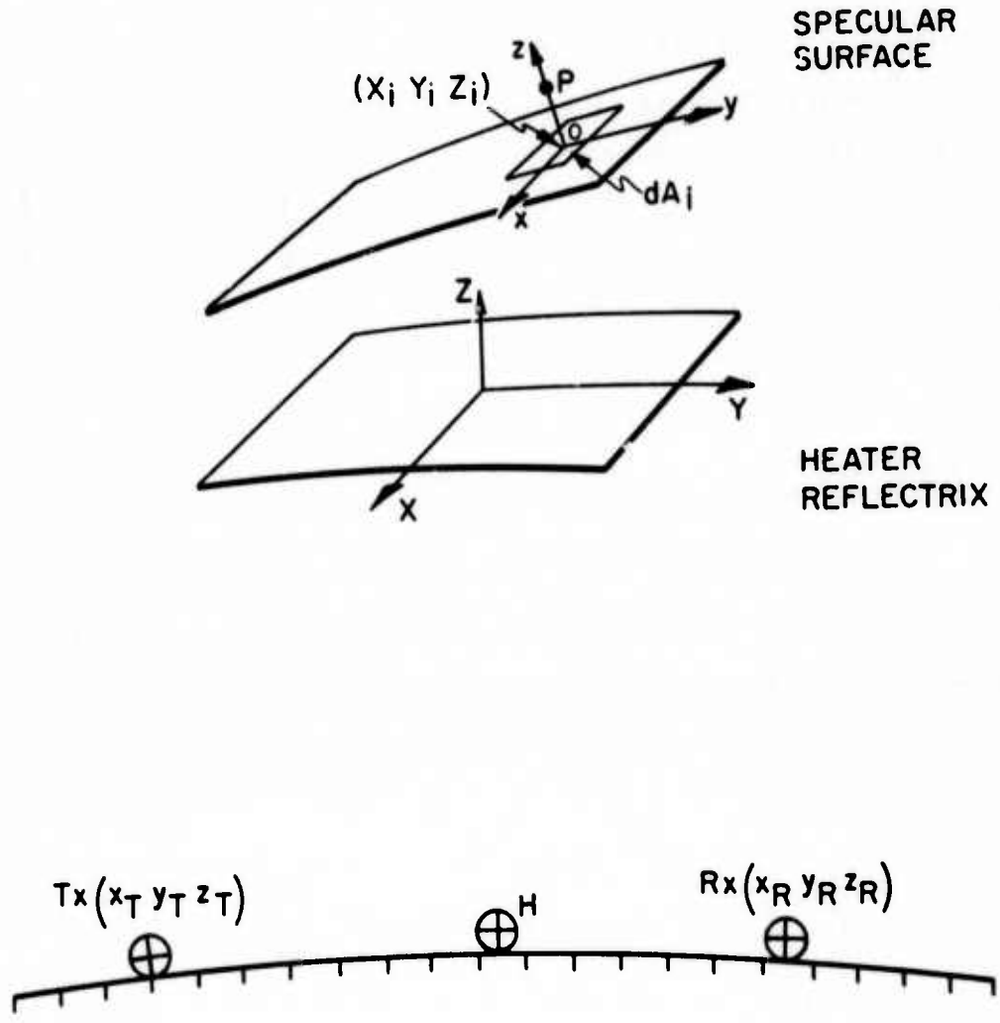

Figure 11. Sketch of Bistatic Radar Geometry showing the coordinate systems on the specular surface and the heater reflectrix used in the model

Where $\overline{(\Delta N/N)^2}_{Ri}$ is the density fluctuation on the reflectrix at a radial distance $R_i = (X_i^2 + Y_i^2)^{\frac{1}{2}}$ and it is determined by the yeild model described earlier. The fluctuation intensity at point P, that is at (0, 0, z) in the system centered on dA_i, is given as:

$$\overline{(\Delta N/N)^2} = \overline{(\Delta N/N)_i^2} \exp - \left\{ \frac{z \cos\gamma}{A} \right\}^2 \tag{21}$$

Where $\gamma = (90 - I)$ and I is the dip angle.

On the assumption of Gaussian spatial correlation, we get for the parallel component of the density spectrum

$$P_{\parallel} \left\{ K (n_2 - n_1) \right\} = (2\pi)^{\frac{1}{2}} L \exp - \left\{ \frac{K^2 L^2 (n_2 - n_1)^2}{2} \right\} \tag{22}$$

using the geometry shown in Figure 12, the direction cosines of the incident and scattered wave vectors can be related to the aspect and scattering angles ψ and ϕ_s as:

$$(n_2 - n_1)^2 = 4 \sin^2 \phi_s/2 \sin^2\psi$$

$$(\ell_2 - \ell_1)^2 + (m_2 - m_1)^2 = 4 \sin^2 \phi_s/2 \cos^2 \psi$$

In the case of strong aspect sensitive scatter, the effective scattering is limited to small values of ψ and we can approximate the above relations to

$$(n_2 - n_1)^2 \approx 4z^2/R'^2 \quad \text{Where } R' = \frac{2R_1 R_2}{(R_1 + R_2)} \tag{23a}$$

and

$$(\ell_2 - \ell_1)^2 + (m_2 - m_1)^2 \approx 4 \sin^2 \phi_s/2 \tag{23b}$$

using equations (21), (22) and (23a, b), we get for (19)

$$\sigma_v = \frac{(2\pi)^{\frac{1}{2}} \pi^2 \sin^2\chi}{\lambda_N^4} \overline{(\Delta N/N)_i^2} L P_{\perp} (2K \sin \phi_s/2)$$

$$\exp \left\{ - \left[\frac{\cos^2\gamma}{A^2} + \frac{2K^2L^2}{R'^2} \right] z^2 \right\} \tag{24}$$

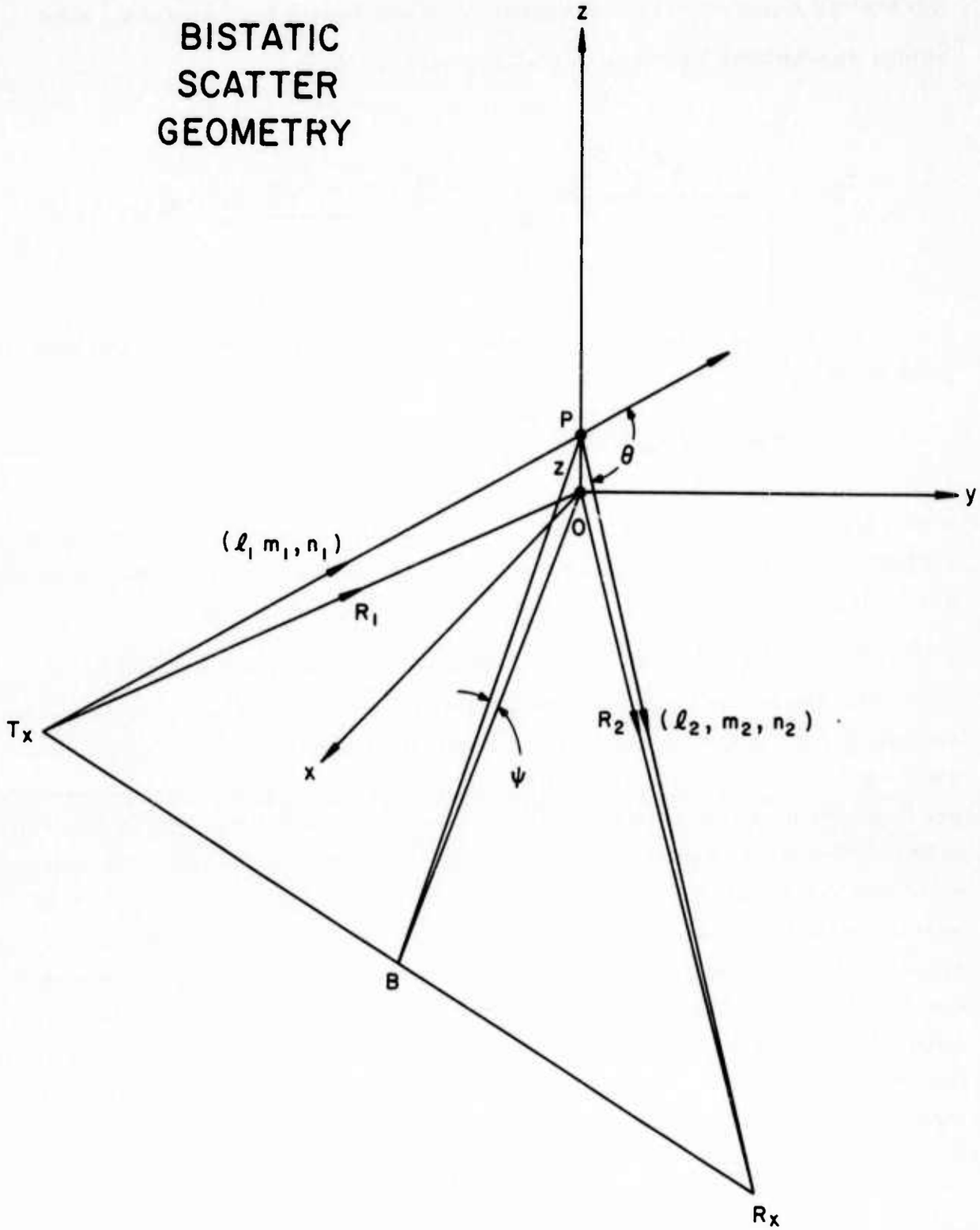

Figure 12. Geometry showing the Relation Between the Direction Cosines and Scattering Angles ψ and ϕ_s. (U)

Integrating Equation (24) with respect to z and letting γ, χ, ϕ_s and λ_N take values appropriate to the center of dA_i will result in

$$\sigma_{Ai} = \left[\frac{\pi^2 \sin^2\chi_i}{1 + \frac{\lambda^2 R'^2 \cos^2\gamma_i}{8\pi^2 L^2 A^2}}\right]^{\frac{1}{2}} \frac{\lambda R'}{2} \frac{\overline{(\Delta N/N)_i^2}}{\lambda_{N_i}^4} P_\perp (2K \sin \phi_{si}/2) \qquad (25)$$

The total cross section is obtained by numerical evaluation of the surface integral of σ_A. Thus

$$\sigma_T = \int_S \sigma_A \, dA = \sum_{i=1}^{i=N} \sigma_{Ai} \, dA_i \qquad (26)$$

where N is the number of elements into which the active region of the specular surface is divided. Figure 13 shows a scheme for computer adaptation of the scattering model.

4B. Special Case (Monostatic Geometry and Idealized Yield Model)

The scattering model for the total cross section can be presented in an analytic form for the special case of a monostatic geometry and an idealized yield model. The solution is of some interest since a general bistatic radar problem can be reduced to an equivalent monostatic case and can be evaluated to a first order without resorting to a complex computer program. The approximate nature of the solution is a consequence of two simplifying assumptions that readily permit an analytic description to the model. The assumptions are that the magnetic field is constant over the dimensions of the scattering volume and that the intensity of the density fluctuations is directly proportional to the power density on the heater reflectrix. Starting with Equation (1) and following the steps given by Pendyala and Thome (1972)[3], we obtain for a pulse radar with a Gaussian pulse length p and beam width B:

$$\sigma_p(K) = \frac{2\pi^4 W^2 \lambda R}{\lambda_N^4} \left(\overline{\frac{\Delta N}{N}}\right)_o^2 M_f \, P_\perp(2K) \frac{1}{\left[\cos^2\theta + \frac{W^2}{A^2} \sin^2\theta + \frac{W^2}{p}\right]^{\frac{1}{2}}} \frac{1}{\left[1 + 2(W/BR)^2\right]^{\frac{1}{2}}} \frac{1}{\left[1 + \delta\right]^{\frac{1}{2}}} \qquad (27)$$

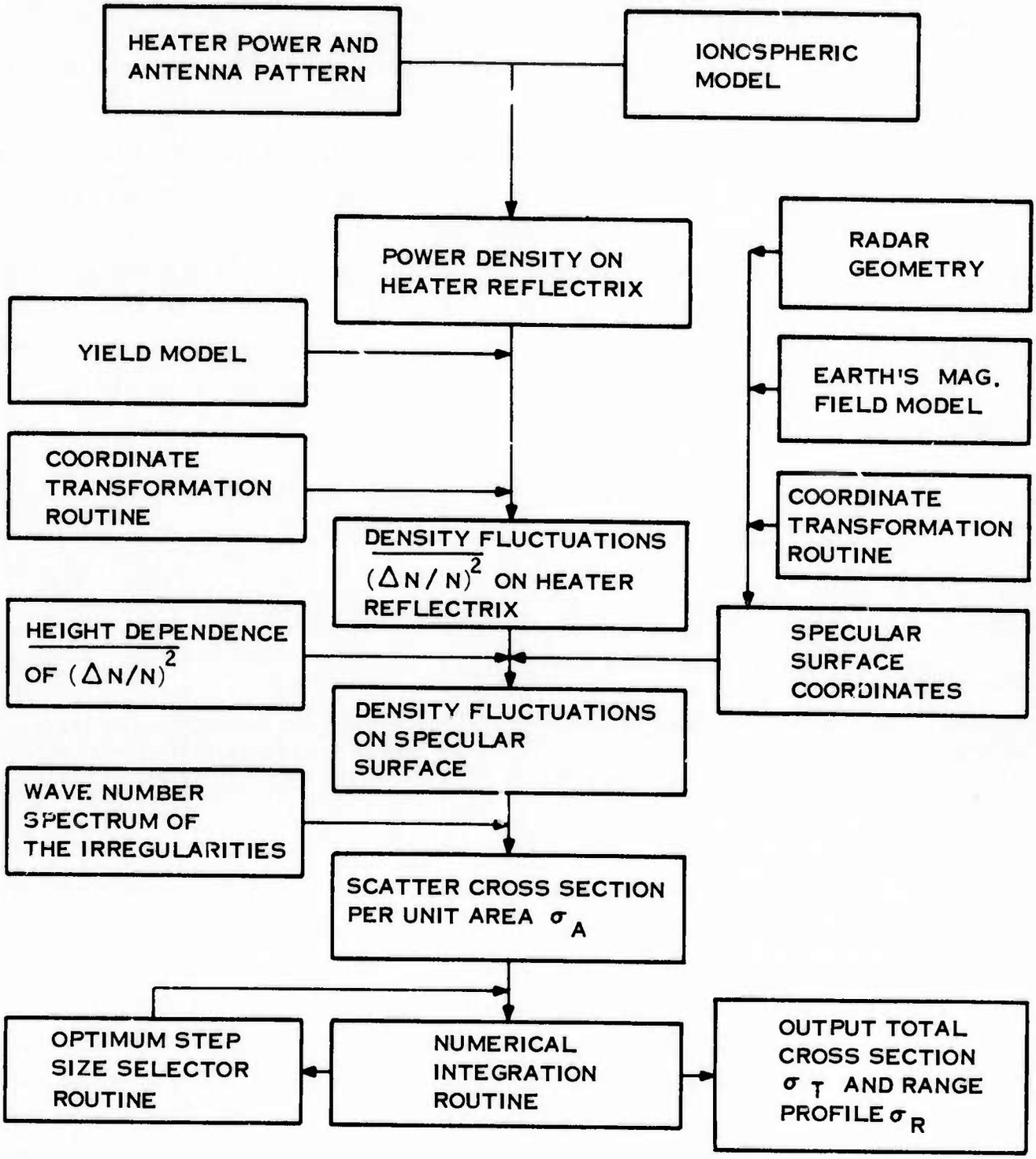

Figure 13. Flow Chart for Computer Adptation of the Model (U)

where M_f is a factor arising due to mismatch between heater reflectrix and specular surface and is given as:

$$M_f = \exp - \left\{ \frac{D^2}{A^2} (1 - \Delta) \right\} \approx \exp - \left\{ D^2/A^2 \right\} \qquad (28)$$

Δ is a function of θ, A, W, p, B and R and is much less than 1 for most cases of interest thus leading to the above approximation. In the case of strong aspect sensitive scattering, $\delta << 1$ further simplifying the equation for σ_p. By letting the pulse length and the beam width to exceed the dimension W of the scattering volume, σ_p can be made to approach the total cross section σ_T. On the basis of the relationship between monostatic and bistatic radar configurations discussed earlier, the total cross section for a bistatic radar illuminating the entire disturbed volume obtains the form:

$$\sigma_T (K) = \frac{2\pi^4 \sin^2 \chi \; W\lambda \; R'}{\lambda_N^4} \left\langle \left(\frac{\Delta N}{N} \right)^2 \right\rangle_o M_f \; P\,(2K \sin \phi_s/2)$$

$$\frac{1}{\left[\cos^2 \theta + (W/A)^2 \sin^2 \theta \right]^{\frac{1}{2}}} \qquad (29)$$

Where ϕ_s is the scattering angle and the equivalent range $R' = 2R_1R_2/(R_1 + R_2)$. The above equation will be useful for the purpose of quick evaluation of a given radar link.

5. MODEL VERIFICATION (U)

According to the model presented above, there will be an enhancement in the radar cross section to be gained by going from monostatic to bistatic configuration when operating in the region where the spectral function $P_\perp(K_T)$ decreases with the increasing wavenumber. A multi-station CW scattering experiment designed to verify the model prediction was conducted by SRI using an operating frequency of 144 MHz that falls in the region of steep slope of the cross section - versus - frequency curve (Frank, et al, 1973).[4] The experiment involves a comparison of the cross sections observed over a near-backscatter path with $\phi_s = 168^\circ$ (Ocotillo-Lancaster) and a forward scatter path with $\phi_s = 89^\circ$ (Ocotillo-Huntsville). The observations show a 10 dB gain in the cross section

for the forward scatter path relative to the backscatter case. The scattering model predicts an enchancement of about 14 dB on the assumption that the polarization and mismatch effects are small. The difference noted between the model prediction and the observation is considered to be within the error bounds of the experiment.

6. CONCLUDING REMARKS (U)

The scattering model presented here deals only with the so called 'on-frequency component of scatter from the heated volume. There are other components (e.g., ion lines and plasma lines), but these are relatively weak and appear to be of secondary importance for applications. The model has been developed on the basis of information available primarily from the field experiments reported to date. In order to place the model on a firmer ground, relevant laboratory and theoretical contributions also need to be incorporated into the model. Although the model is based upon the observations limited to the conditions of ordinary mode heating of the daytime F-region, the underlying concepts apply as well to any other situation where the scattering mechanism is identified to be the same. Specifically, the model needs to be extended for the E region and the nighttime heating conditions.

APPENDIX

DETERMINATION OF SPECULAR SURFACE (U)

(U) The specular surface is defined by a region of points where the external bisector to the angle between the incidence and scattering directions achieves perpendicularity to the direction of the earth's magnetic field. The determination of the specular surface within the volume of the scattering medium for a given radar configuration is one of the main modeling tasks. An analytic solution was obtained to the problem for the case of curved earth and dipole model for the earth's magnetic field but neglecting the ionospheric refraction effects. The solution provides the height of a specular point for a specified location on earth and it results from a cubic equation which is formulated by equating the angle between the incident ray and the magnetic field to that between the scattered ray and the magnetic field.

The solution was adopted to a CDC 6700. The computer output for a specified radar geometry and heater location is a matrix of 325 specular heights calculated at equally spaced intervals within a region of 180 Km square centered over the heater. Figure 14 shows a specimen display generated for the case of Los Lunas - Soccorro radar path and Platteville heater. The program can compute and display the ranges from the transmitter and receiver to each of the 325 specular points in space if so desired. A more general program has been developed at SRI to compute the specular surface which takes the ionospheric refraction effects also into account.

LOS LUNAS (34.798°N, 106.66°W) - SOCORRO (33.963°N, 106.889°W)

SPECULAR HEIGHT

DIS(KM)	LONG	-90.00	-75.00	-60.00	-45.00	-30.00	-15.00	.00	15.00	30.00	45.00	60.00	75.00	90.00	
	LAT	254.23	254.41	254.58	254.75	254.92	255.09	255.27	255.44	255.61	255.78	255.96	256.13	256.30	
90.00	40.96	251.37	252.31	253.20	254.02	254.78	255.47	256.10	256.66	257.16	257.59	257.96	256.27	258.51	40.96
82.50	40.89	250.04	250.99	251.88	252.70	253.46	254.15	254.78	255.35	255.85	256.29	256.66	256.97	257.21	40.89
75.00	40.83	248.69	249.64	250.53	251.36	252.12	252.81	253.45	254.01	254.52	254.96	255.33	255.64	255.89	40.83
67.50	40.76	247.32	248.27	249.17	249.99	250.76	251.46	252.09	252.66	253.17	253.61	253.99	254.30	254.55	40.75
60.00	40.70	245.93	246.88	247.78	248.61	249.37	250.07	250.72	251.29	251.80	252.24	252.62	252.94	253.19	40.70
52.50	40.63	244.52	245.47	246.37	247.20	247.97	248.68	249.32	249.89	250.40	250.85	251.23	251.55	251.80	40.63
45.00	40.57	243.08	244.05	244.94	245.78	246.55	247.26	247.90	248.48	248.99	249.44	249.82	250.14	250.40	40.57
37.50	40.50	241.63	242.59	243.50	244.33	245.11	245.81	246.46	247.04	247.55	248.01	248.39	248.72	248.98	40.50
30.00	40.44	240.15	241.12	242.03	242.87	243.64	244.35	245.00	245.58	246.10	246.55	246.95	247.27	247.53	40.44
22.50	40.37	238.66	239.63	240.53	241.38	242.15	242.87	243.52	244.11	244.63	245.08	245.47	245.80	246.06	40.37
15.00	40.31	237.14	238.11	239.02	239.87	240.65	241.37	242.02	242.61	243.13	243.59	243.98	244.31	244.58	40.31
7.50	40.24	235.60	236.58	237.49	238.34	239.12	239.84	240.49	241.09	241.61	242.07	242.47	242.80	243.07	40.24
.00	40.18	234.04	235.02	235.94	236.79	237.57	238.29	238.95	239.54	240.07	240.54	240.94	241.27	241.54	40.18
-7.50	40.11	232.46	233.45	234.36	235.22	236.00	236.73	237.39	237.98	238.51	238.98	239.38	239.72	239.99	40.11
-15.00	40.05	230.86	231.85	232.77	233.62	234.41	235.14	235.80	236.40	236.93	237.40	237.81	238.15	238.42	40.05
-22.50	39.98	229.24	230.23	231.15	232.01	232.80	233.53	234.19	234.79	235.33	235.80	236.21	236.55	236.83	39.98
-30.00	39.92	227.60	228.59	229.51	230.37	231.17	231.90	232.57	233.17	233.71	234.16	234.59	234.94	235.22	39.92
-37.50	39.85	225.93	226.92	227.85	228.71	229.51	230.25	230.92	231.52	232.06	232.54	232.95	233.30	233.58	39.85
-45.00	39.79	224.24	225.24	226.17	227.04	227.84	228.58	229.25	229.86	230.40	230.88	231.29	231.65	231.93	39.79
-52.50	39.72	222.54	223.53	224.47	225.34	226.14	226.88	227.55	228.17	228.71	229.19	229.61	229.97	230.25	39.72
-60.00	39.66	220.81	221.81	222.74	223.62	224.42	225.17	225.84	226.46	227.01	227.49	227.91	228.27	228.56	39.66
-67.50	39.59	219.06	220.06	221.00	221.87	222.68	223.43	224.11	224.72	225.28	225.76	226.19	226.55	226.84	39.79
-75.00	39.53	217.28	218.29	219.23	220.11	220.92	221.67	222.35	222.97	223.53	224.02	224.44	224.81	225.10	39.53
-82.50	39.46	215.49	216.50	217.44	218.32	219.14	219.89	220.58	221.20	221.76	222.25	222.68	223.04	223.34	39.46
-90.00	39.40	213.68	214.69	215.63	216.52	217.33	218.09	218.78	219.40	219.97	220.46	220.89	221.26	221.56	39.40
	LONG	254.26	254.43	254.59	254.76	254.93	255.10	255.27	255.44	255.60	255.77	255.94	256.11	256.28	

Figure 14. A Sample Display of Specular Height Matrix above Platteville Heater for Los Lunas - Soccorro Radar path

REFERENCES (U)

1. H. G. Booker, "A Theory of Scattering by Nonisotropic Irregularities with Application to Radar Reflections from the Aurora (U)", J. Atmos. Terr. Phys., Vol. 8, pp 204-221 (1956), UNCLASSIFIED

2. J. Minkoff, "Analysis and Interpretation of Aspect-Dependent Ionospheric Radar Scatter (U)", J. G. R., Vol. 78, No. 19, pp 3865-3880 (1973), UNCLASSIFIED

3 & 4. These references available to qualified military and government agencies on request from RADC (OCSE), GAFB, NY 13441.

MISSION
of
Rome Air Development Center

RADC is the principal AFSC organization charged with planning and executing the USAF exploratory and advanced development programs for electromagnetic intelligence techniques, reliability and compatibility techniques for electronic systems, electromagnetic transmission and reception, ground based surveillance, ground communications, information displays and information processing. This Center provides technical or management assistance in support of studies, analyses, development planning activities, acquisition, test, evaluation, modification, and operation of aerospace systems and related equipment.